ADVANCED FUNCTIONAL MATERIALS
www.afm-journal.de

Tunable and Recyclable Piezoelectric Biomaterials via Ion-Directed Guanine-Quadruplex Assembly

Seungho Lee, Sangyun Na, Yumi Cho, Gaeun Park, Seung Hak Oh, Jaejun Kim, Byoung-Ki Cho, Sang Kyu Kwak, Ja-Hyoung Ryu,* and Hyunhyub Ko**

The self-assembly of biomaterials into piezoelectric architecture offers a promising pathway toward sustainable and functional alternatives to conventional piezoelectric materials. Herein, guanine-quadruplex (GQ) structures are introduced as a new class of self-assembled biomolecular piezoelectric materials, formed via facile ion-mediated assembly of amphiphilic guanine derivatives in the presence of alkali metal ions (Li^+, Na^+, and K^+). Through a combination of molecular dynamics (MD) simulations and experimental validation, an ion-specific piezoelectric mechanism is uncovered, wherein K^+-assembled GQs show the highest dipole distortion and piezoelectric output due to favorable ionic positioning within the GQ columnar channel. Notably, the system allows facile tuning of piezoelectric performance by simply varying the coordinating ion and demonstrates excellent recyclability through a one-step dissolution–evaporation process. This work establishes a versatile and eco-friendly platform for developing tunable, recyclable piezoelectric materials for next-generation bioelectronic applications.

1. Introduction

Piezoelectric materials generate electricity in response to mechanical deformation, a phenomenon originating from the displacement of internal dipoles within non-centrosymmetric structures.[1–3] This fundamental mechanism linking mechanical deformation to electrical output enables them to function as transducers that convert mechanical stimuli such as pressure,[4,5] strain,[6,7] or vibration[8] into electrical signals and vice versa. Owing to these properties, piezoelectric materials are widely employed in diverse applications, including energy harvesting,[9] wearable electronics,[10] and acoustic devices.[11] Among various candidates, fluoropolymer-based materials have been widely used in flexible piezoelectric devices due to their strong dipole moments arising from the difference in electronegativity between fluorine and hydrogen atoms.[12–14] However, their limited biodegradability and toxicity present significant challenges for environmental sustainability.[15,16]

To overcome the environmental limitations of conventional piezoelectric materials, biomolecule-based alternatives have gained increasing attention due to their inherent environmental sustainability and biocompatibility.[17–20] For example, smaller building blocks such as amino acids in chiral symmetry groups,[21,22] collagen,[23,24] and nucleotides[25] have been reported to exhibit inherent piezoelectric properties. Meanwhile, highly organized supramolecular architectures can induce collective dipole alignment, as demonstrated in assemblies of amino acid[26,27] and peptide[28,29] and protein-based fibrils.[30,31] Through precise control of the assembled structure, these systems form highly ordered architectures that enhance both thermal stability and dipole alignment.[32]

Although significant progress has been made in engineering self-assembled structures to enhance piezoelectric performance, most existing systems still exhibit limited tunability in their piezoelectric properties. Achieving tunability often requires altering finely optimized fabrication parameters, such as solvent composition[33] or synthetic method,[34] to obtain a specific supramolecular architecture, which in turn limits adaptability across diverse operational environments with varying performance demands. Furthermore, these complex and condition-sensitive assembly processes hinder material recyclability, often

S. Na, Y. Cho, S. H. Oh, J. Kim, H. Ko
School of Energy and Chemical Engineering
Ulsan National Institute of Science and Technology (UNIST)
Ulsan 44919, Republic of Korea
E-mail: hyunhko@unist.ac.kr
S. Lee, G. Park, J.-H. Ryu
Department of Chemistry
Ulsan National Institute of Science and Technology (UNIST)
Ulsan 44919, Republic of Korea
E-mail: jhryu@unist.ac.kr
B.-K. Cho
Department of Chemistry
Dankook University
Cheonan 31116, Republic of Korea
S. K. Kwak
Department of Chemical and Biological Engineering
Korea University
Seoul 02841, Republic of Korea
E-mail: skkwak@korea.ac.kr

The ORCID identification number(s) for the author(s) of this article can be found under https://doi.org/10.1002/adfm.202517112

DOI: 10.1002/adfm.202517112

requiring stimulus-specific[35] or time-consuming[36] reassembly steps, thereby compromising practical deployment and cost-effectiveness.

Guanine-quadruplexes (GQs) are secondary DNA structures formed by assembly of guanine-rich sequences.[37] Through robust supramolecular interactions, including Hoogsteen hydrogen bonding, cation-dipole interactions, and π-π stacking[38–41] GQs exhibit enhanced thermal stability. Specifically, Hoogsteen hydrogen bonding between guanine bases gives rise to planar G-quartets, which stack vertically through π–π interactions to form a stable columnar core. Monovalent cations coordinated within the central channel further stabilize the structure by neutralizing electrostatic repulsion between the inward-oriented guanine oxygens.[42,43] In addition, GQ structure can be simply regulated by the type of alkali metal ions incorporated, offering tunable structural control.[44,45] Although GQs are biomaterial-based structures with excellent thermal stability and ion-tunability, their structural symmetry[46,47] may have limited the exploration of their piezoelectric properties, which remain largely uninvestigated.

Herein, we report the first demonstration of piezoelectric behavior in GQ structures, assembled via alkali ion-mediated self-assembly of an amphiphilic guanine derivative (Molecule 1, **Figure 1**a). This fan-shaped molecule, featuring a lipophilic trialkoxybenzyl group at the N9 position of guanine, is designed to promote mesogenic organization into either GQ or dimeric structures depending on the presence of alkali metal ions (Li^+, Na^+, or K^+).[48] In the presence of these cations, molecule 1 undergoes cation-directed self-assembly into well-defined GQ complexes—designated as 1-Li, 1-Na, and 1-K—via specific supramolecular interactions (Figure 1b). Through a combination of molecular dynamics (MD) simulations and experimental characterization, we uncover a unique ion-specific mechanism underlying the piezoelectric response: smaller Li^+ ions occupy intralayer sites within the GQ stack, while larger Na^+ and K^+ ions localize at interlayer positions. Upon mechanical deformation, the entire GQ structure undergoes compression, resulting in reduced interlayer spacing and rearrangement of both the G-quartet framework and the coordinated cations (Figure 1c). Under pressure, K^+ and Na^+ ions largely remain confined within the GQ columnar channel and exhibit pressure-aligned, collective movement along the stacking direction. In contrast, the smaller Li^+ ions with larger voids tend to deviate laterally from the channel under compression, showing more random and uncoordinated motion, which leads to less stable and disordered structural rearrangement. Together with the reorientation of distributed atomic dipoles and ion displacement, a net change in dipole moment along the stacking axis ($\Delta\mu_z$) is induced, which generates an electric potential and subsequently drives the piezoelectric current. Furthermore, we demonstrate that the GQ-based piezoelectric devices can be easily recycled through a simple dissolution–evaporation process, with full recovery of their sensing performance across multiple cycles (Figure 1d). Taken together, this work introduces a novel class of biomolecular piezoelectric materials that enable facile ion-dependent tunability and solvent-assisted recyclability. Without requiring complex synthetic procedures or precise condition control, both piezoelectric performance and material reuse can be easily achieved, offering strong potential for sustainable and scalable integration into next-generation bioelectronic systems.

2. Results and Discussion

2.1. Ion-Dependent Self-Assembly of GQ Structures

Self-assembled GQ structures were obtained by adding alkali metal cations to molecule 1 dissolved in chloroform (Figures S1–S6, Supporting Information). Notably, chloroform provided higher solubility for the self-assembled GQ complex than dimethylformamide (DMF), although both solvents showed low solubility for molecule 1 alone (Figure S7, Supporting Information). The enhanced solubility is attributed to the hydrophobic effect of the amphiphilic molecule, which facilitates different self-assembly behavior. Depending on the presence of cations, molecule 1 self-assembles into distinct structures through different hydrogen bonding patterns: a dimeric structure without cations (**Figure 2**a i) and a GQ structure with cations (Figure 2a ii). Gel permeation chromatography (GPC) traces revealed sharp peaks at retention times <8 min for the GQ complexes, in contrast to the broader peak of molecule 1 at >8 min (Figure 2b), indicating increased molecular size upon self-assembly. Among the complexes, 1-K exhibited the highest molecular weight, followed by 1-Na and 1-Li, reflecting differences in the supramolecular interactions specific to each cation.[40]

Solvent-dependent self-assembly behavior was investigated via ^{1}H nuclear magnetic resonance (NMR) spectroscopy. As shown in Figure 2c, molecule 1 dissolved in dimethyl sulfoxide (DMSO-d_6) exhibits minimal changes in cation-dependent chemical shift, suggesting limited intermolecular interactions owing to the high solubility of both the guanine moiety and the added salts in the polar solvent. Under these conditions, molecule 1 remains mostly unassembled, with hydrogen bonding between molecule 1 and ion-dipole interactions with added cations effectively suppressed. In contrast, chloroform enables cation-induced self-assembly, as evidenced by cation-dependent chemical shift variations (Figure 2d). Specifically, the formation of Hoogsteen hydrogen bonds and reduced intermolecular distances in the self-assembled structures lead to an upfield shift of the N1H resonance compared to molecule 1 (at 12.2 ppm). As the ionic radius increases from Li^+ to Na^+ to K^+, the N1H resonance becomes increasingly split and shifts slightly downfield, reflecting more heterogeneous local environments. Similar splitting patterns are observed for the N2H, C8H, and N9CH protons, indicating progressively more complex supramolecular assemblies with increasing cation size.[49]

Diffusion-ordered spectroscopy (DOSY) NMR analysis revealed a decreasing trend in diffusion coefficients in the order of 1, 1-Li, 1-Na, and 1-K, indicating progressively larger self-assembled structures (Figure 2e). Based on these values, the relative assembly sizes are estimated as dimer, 4-mer, 8-mer, and 16-mer complexes for 1, 1-Li, 1-Na, and 1-K, respectively.[50,51] These results confirm that amphiphilic guanine derivatives form self-assembled GQ structures through cation-dependent self-assembly in polar aprotic solvents. Such solvents play a critical role by dissolving ionic species while preserving the hydrogen-bonding capability of guanine moieties, thereby facilitating

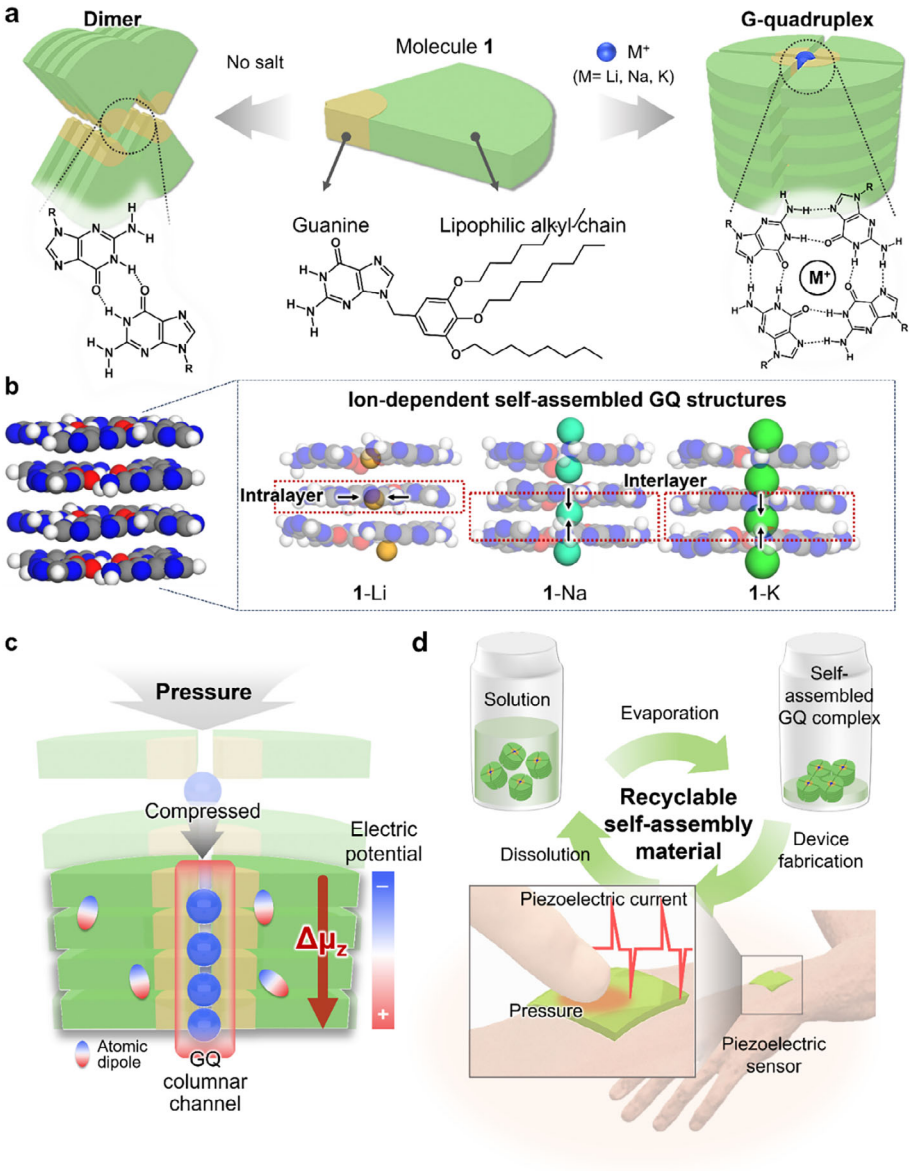

Figure 1. Ion-dependent self-assembly and piezoelectric behavior of GQ complexes formed from amphiphilic guanine and alkali metal ions. a) Chemical structure of the guanine derivative (molecule 1) and its self-assembled structures: dimer (without ions) and G-quadruplex (with alkali metal ions). b) Cation-dependent self-assembly of GQ complexes (1-Li, 1-Na, 1-K), showing distinct ion positions: Li^+ within G-quartet layers (intralayer) and Na^+/K^+ between layers (interlayer). c) Schematic of the piezoelectric mechanism in GQ complexes. External pressure induces structural rearrangement, and dipole reorientation generates a net dipole moment change ($\Delta\mu_z$), forming an electric potential. d) Recyclable and wearable piezoelectric sensor fabricated using the self-assembled GQ complex.

directional supramolecular interactions essential for GQ formation. Additionally, the structural complexity of the resulting assemblies is strongly influenced by the specific identity of the alkali cation.

2.2. Liquid Crystalline Properties of GQ Complexes

The fan-shaped guanine derivative (molecule 1) was designed to maintain a stable GQ structure even after solvent evaporation. This feature was assessed by preparing liquid crystalline GQ complexes via slow evaporation of chloroform. Magic angle spinning (MAS) ^{1}H NMR analysis revealed changes in N1H resonance associated with Hoogsteen hydrogen bonding, consistent with the trends in solution-state NMR (Figure 2f). In molecule 1, the N1H signal appears above 14 ppm, characteristic of a ribbon-like structure (indicated by "R"), but shifts to below 12 ppm upon cation addition, indicating the formation of a GQ structure (indicated by "Q").[51,52] These cation-dependent shifts confirm the presence of Hoogsteen hydrogen bonds and the formation of distinct GQ structures regulated by the type of alkali metal ion. Notably, similar resonance trends in both solution and liquid

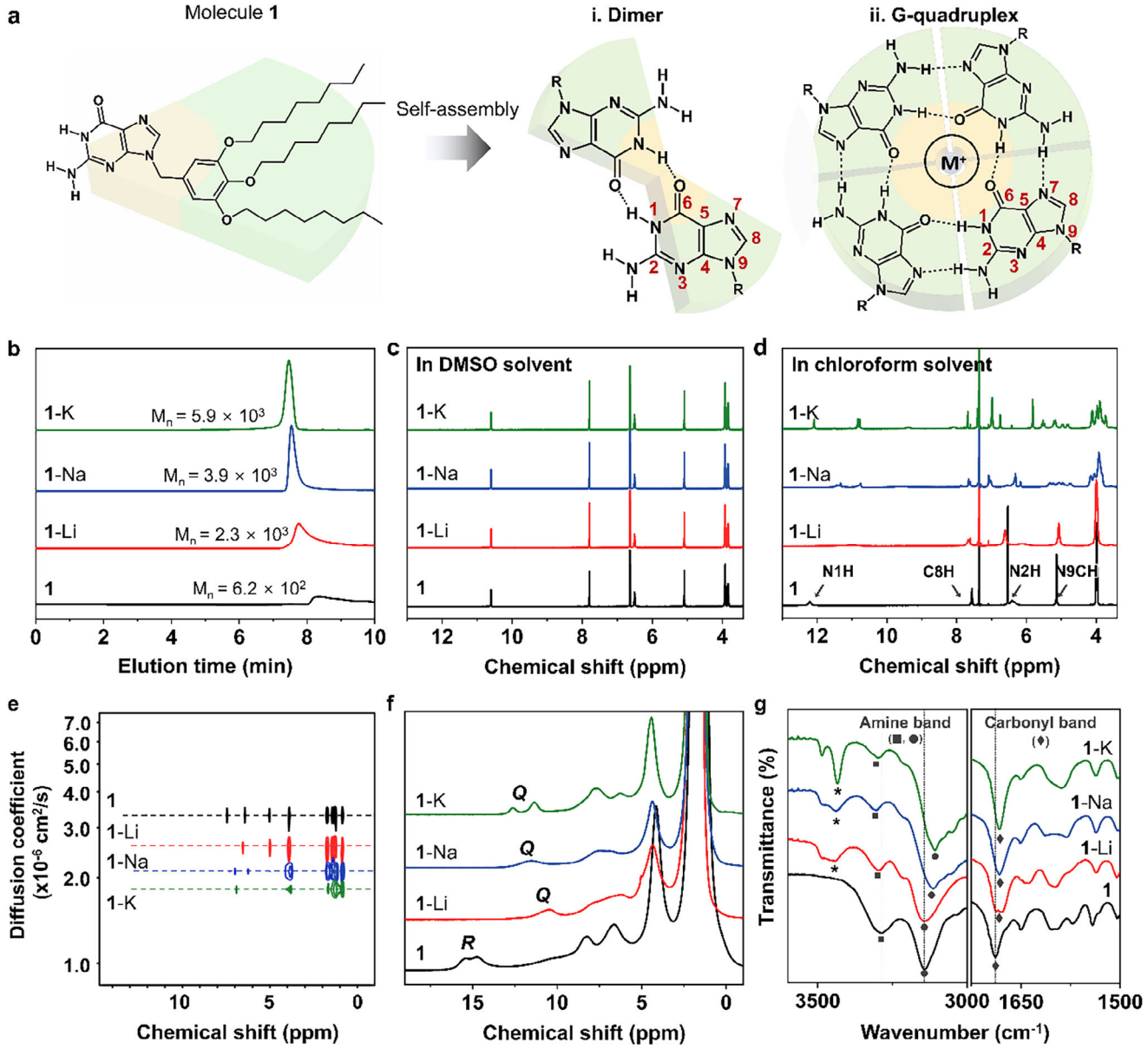

Figure 2. Characterization of GQ complexes. a) Chemical structures of amphiphilic guanine derivative (molecule 1) and its self-assembled forms: dimer (left) and GQ (left) via alkali metal ion coordination. b) GPC traces of 1 (black), 1-Li (red), 1-Na (blue), and 1-K (green) in $CHCl_3$, showing increased molecular size upon GQ formation. c, d) Solution ^1H NMR spectra of 1 and GQ complexes in (c) DMSO-d6 and (d) $CDCl_3$, highlighting ion-induced chemical shift variations. e) DOSY NMR data of 1 and GQ complexes in $CDCl_3$, showing decreased diffusion coefficients with increasing GQ assembly size. f) Solid-state MAS ^1H NMR spectra showing distinct N1H resonances for different assemblies (R: Ribbon-like structure). g) FTIR spectra in the solid state indicate formation of Hoogsteen hydrogen bonds and cation-dependent band shifts in amine and carbonyl regions.

crystalline states demonstrate that the GQ structure is preserved even after solvent removal.

Fourier-transform infrared (FTIR) spectra of GQ complexes in the liquid crystalline phase (Figure 2g) reveal changes in transmission bands related to functional groups involved in Hoogsteen hydrogen bonding. Upon cation addition, the amine bands at 3287 cm^{-1} (■) and 3149 cm^{-1} (●), as well as carbonyl bands at 1689 cm^{-1} (♦), shift, indicating the formation of self-assembled GQ-structures. Additionally, a new peak appears at ≈3440 cm^{-1} (*), while the N2 peak at 3300 cm^{-1} diminishes, which is attributed to the formation of new hydrogen bonds between N2-H and N7. The new peak at 3440 cm^{-1} becomes increasingly sharp in 1-K, suggesting enhanced structural ordering and stability with larger cations.

The designed fan-shaped molecules initially self-assemble into disk-shaped G-quartet units, which further stack into columnar GQ structures. These self-assembled GQ complexes exhibit liquid crystalline properties, as confirmed by wide-angle X-ray scattering (WAXS) and polarized light microscopy (POM). The phase type is tunable by the choice of cation species. WAXS analysis

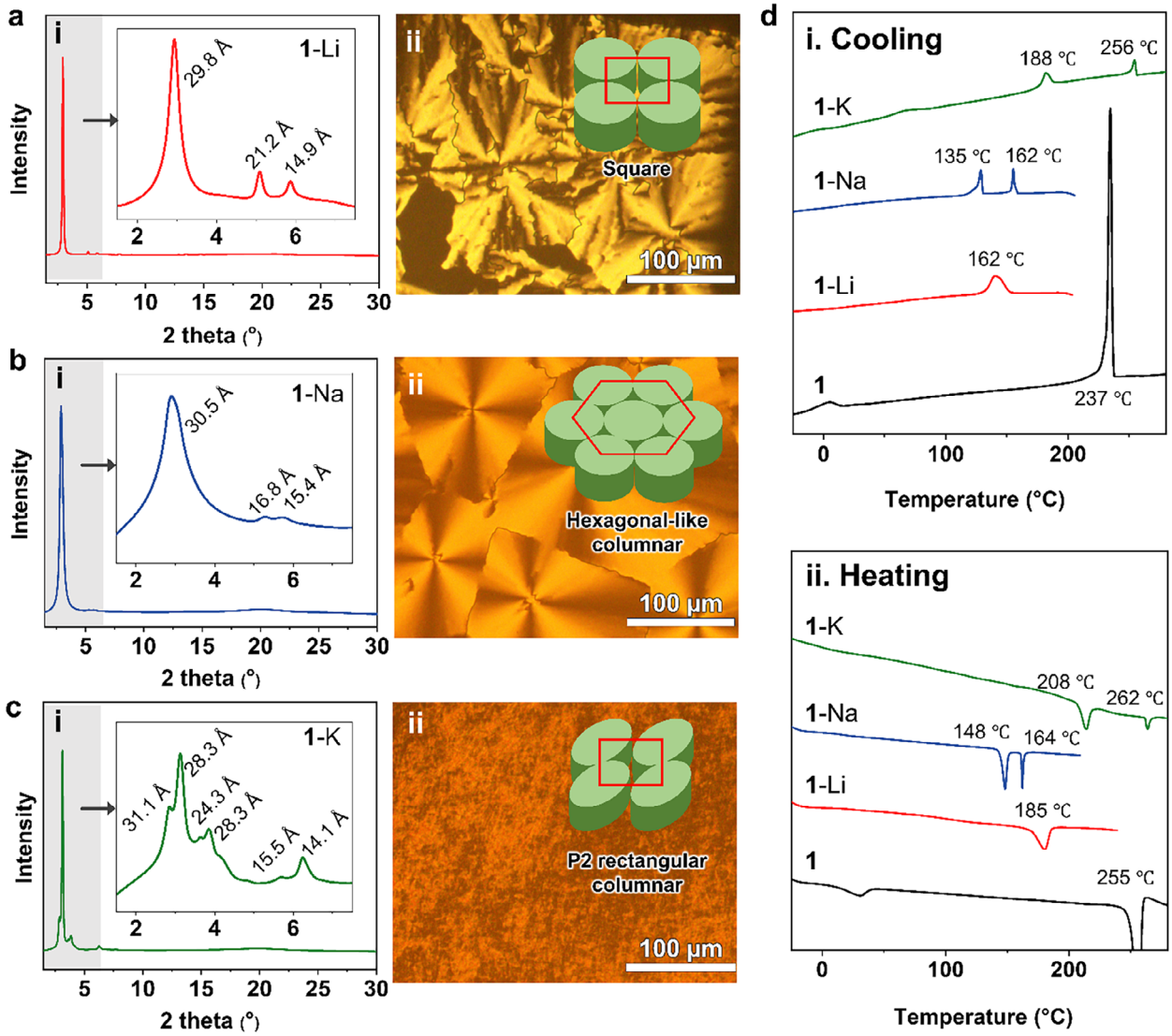

Figure 3. Structural and thermotropic properties of GQ complexes. a–c) WAXS profiles (i) and POM images (ii) of 1-Li (a), 1-Na (b), and 1-K (c) after solvent evaporation, showing square, hexagonal-like, and P2 rectangular columnar phases, respectively. Insets show log-scale plots of the Y axis. d) DSC profiles of molecule 1, 1-Li, 1-Na, and 1-K during the 1st cooling (i) and 2nd heating (ii) cycles.

of 1-Li indicates a square columnar phase with peaks at 29.8 Å (100), 21.2 Å (110), and 14.9 Å (200) (**Figure 3**a i), with corresponding birefringent textures observed in POM (Figure 3a ii). 1-Na exhibits a hexagonal-like columnar phase with peaks at 30.5 Å (100), 16.8 Å (110), and 15.4 Å (200) (Figure 3b i,ii), while 1-K shows a more complex P2 rectangular columnar structure, with multiple diffraction peaks at 31.1 Å (100), 28.3 Å (10-1), 24.3 Å (001), 22.9 Å (010), 15.5 Å (200), and 14.1 Å (-102) (Figure 3c i,ii). The variation in packing symmetry and interlayer spacing among the stacked G-quartets arises from cation-specific ion-dipole interactions between each alkali metal ion and molecule 1. Notably, 1-K exhibits tilted columnar phases, reflecting stronger coordination between K^+ ions and the GQ core, where enhanced ion–dipole interactions[49] induce lateral offset between stacked G-quartets[52] and promote tilted molecular alignment. These structural features, together with the preservation of ordered stacking observed by MAS NMR and FTIR after solvent evaporation, confirm the formation of thermotropic columnar liquid crystalline phases in the GQ complexes. Additionally, XRD results show that molecule 1 in chloroform shows a crystalline phase, while GQ complexes formed with alkali metal ions exhibit mesogenic phases (Figure S8a, Supporting Information). In contrast, no GQ formation is observed in dimethylformamide (DMF), even with alkali metal ion addition, and all samples display similar crystalline patterns (Figure S8b, Supporting Information). Differential scanning calorimetry (DSC) further confirms the thermal reversibility of the mesophase, with phase transitions occurring above the isotropic temperature (Figure 3d). Remarkably, the GQ structures remain intact at temperatures well above the typical DNA denaturation point (≈80 °C),[53] demonstrating

exceptional thermal stability and suitability for applications in wearable electronics.

2.3. Theoretical Analysis of GQ Structure

To elucidate the piezoelectric effect of the self-assembled GQ structure at the molecular level (i.e., 8 layers of G-quartets), we performed molecular mechanics (MM) and molecular dynamics (MD) simulations. MM simulations were employed to determine the energetically stable configurations of stacked G-quartets, while MD simulations were used to evaluate the changes in the dipole moment under mechanical stress (see *Simulation details*). Upon vertical compression, each self-assembled GQ complex exhibited a collective displacement from its initial position, resulting in distortion of the G-quartet structure and corresponding change in the net dipole moment (**Figure 4a**; Figure S10, Supporting Information). These dipole moment variations, which induce surface polarization, generate internal electric fields.[54] In particular, the reorientation of the dipole vector plays a crucial role in the piezoelectric response. Mechanical pressure induces not only structural torsion, but also dipole alignment.[55–57] This reorientation of the dipole contributes to internal polarization, leading to electrostatic potential gradients and the emergence of an electric signal. Thus, the magnitude of the signal is directly related to the degree of reorientation: the greater the torsion, the stronger the induced electric field. In short, the orientation and angular deviation of the dipole moment vector are key factors in determining piezoelectric strength.

When the z-direction of $\Delta\mu$ in the system before and after compression was checked, 1-Li and 1-Na systems showed the $+z$ direction, whereas the 1-K system showed the $-z$ direction (Figure 4b). The result was drawn from the increase and decrease trend of $\cos(\theta)$ of the relaxed and compressed systems (Figure 4c). If θ is stable over time, the net dipole moment in that direction can be considered invariant during compression. In the case of 1-Li, there were changes in the z and y dipole moments; in the case of 1-Na, only the z dipole moment changed; in the case of 1-K, there were changes in the dipole moments in all three directions. When these changes were calculated comprehensively, 1-K showed the largest (Figure 4d). This result showed a good agreement with the order of the piezoelectric signals in the experiment. Additionally, a peculiar observation was that in the relaxed system, if the metal ions were in the intralayer, the net dipole moments were displaced from the orthogonal axes (i.e., 1-Li). This suggested a disordered alignment of the atomic dipole moments. However, if the metal ions were in the interlayer (i.e., 1-Na and 1-K), the net dipole moments were close to the orthogonal axes, indicating a slightly more ordered state. This orderness did not change even under large pressure, which suggested that the initial alignment of polarizations could affect the increase in piezoelectricity.

2.4. Piezoelectric Sensor of GQ Complex

To experimentally validate the simulated piezoelectric behavior, a GQ-based piezoelectric sensor (thickness of 100 µm) was fabricated by sandwiching the GQ complex between two copper electrodes, followed by thermal annealing below the isotropic transition temperature (Figure S12, Supporting Information). Upon application of mechanical pressure, the interlayer spacing within the GQ stack decreases, inducing structural deformation (**Figure 5a**). This deformation reorients the distributed atomic dipoles within the G-quartet layers, resulting in a net dipole moment change ($\Delta\mu$) along the z-axis and thereby generating a measurable piezoelectric current. Piezoresponse force microscopy (PFM) measurements, performed on a thicker GQ film (300 µm) to obtain a stable signal, revealed that cation-induced GQ formation significantly enhances the piezoresponse (Figure S13, Supporting Information). The measured PFM amplitude (µV) was converted to vertical displacement (pm) using the tip sensitivity factor (33.333 V μm^{-1}), and the resulting displacement values were subsequently used to calculate the piezoelectric coefficient (d_{33}) (Figure 5b). Among the complexes, 1-K exhibited the highest piezoelectric coefficient (d_{33} = 1.9 pm V^{-1}), followed by 1-Na (d_{33} = 0.9 pm V^{-1}) and 1-Li (d_{33} = 0.5 pm V^{-1}). In contrast, the cation-free guanine complex demonstrated negligible piezoresponse (d_{33} = 0.2 pm V^{-1}, Figure S14, Supporting Information) and no signal reversal under polarity-switching conditions (Figure S15a,b, Supporting Information), indicating the absence of piezoelectricity and underscoring the critical role of the GQ architecture in enabling piezoelectric behavior. Piezoelectric current density measurements under mechanical deformation revealed that 1-K produces the highest output, followed by 1-Na and 1-Li (Figure 5c). This trend is consistent with both the simulated changes in dipole moment ($\Delta\mu$) along the z-axis and the experimentally determined piezoelectric coefficients. The superior piezoelectric current observed in 1-K is attributed to the larger K^+ ions promoting more ordered and collective dipole reorientation through tighter packing in the GQ stack, as revealed by MD simulations. In contrast, the smaller Li^+ ions in 1-Li generate relatively more void space within the GQ stack, leading to more random displacement of ions and a less effective net dipole change. Furthermore, the piezoelectric voltage of 1-K increases proportionally with applied pressure (Figure S16, Supporting Information), while 1-Li exhibits minimal dipole change between compression and release, leading to weak and unstable signals under high pressure (Figure S17, Supporting Information).

Unlike conventional covalently bonded polymers, the self-assembled GQ complex exhibits exceptionally facile recyclability, enabling repeated reuse in device fabrication with minimal processing. The supramolecular nature of the GQ structure allows it to be rapidly disassembled—fully dissolving in chloroform within 5 min (Figure 5d)—and spontaneously reassembled upon simple solvent evaporation, without the need for additional reagents or complex processing steps. This rapid and reversible recycling process not only simplifies device manufacturing but also enhances the material's versatility for diverse fabrication environments. Furthermore, the GQ complex can be reprocessed through mild treatments such as sonication (Figure S18, Supporting Information), reinforcing its operational flexibility. Notably, the piezoelectric performance remains stable across the as-prepared, 1st, and 2nd recycled samples (Figure 5e), highlighting a key advantage for sustainable and recyclable device applications. The GQ-based piezoelectric sensor exhibits excellent operational stability under standard conditions, maintaining consistent current output over 5000

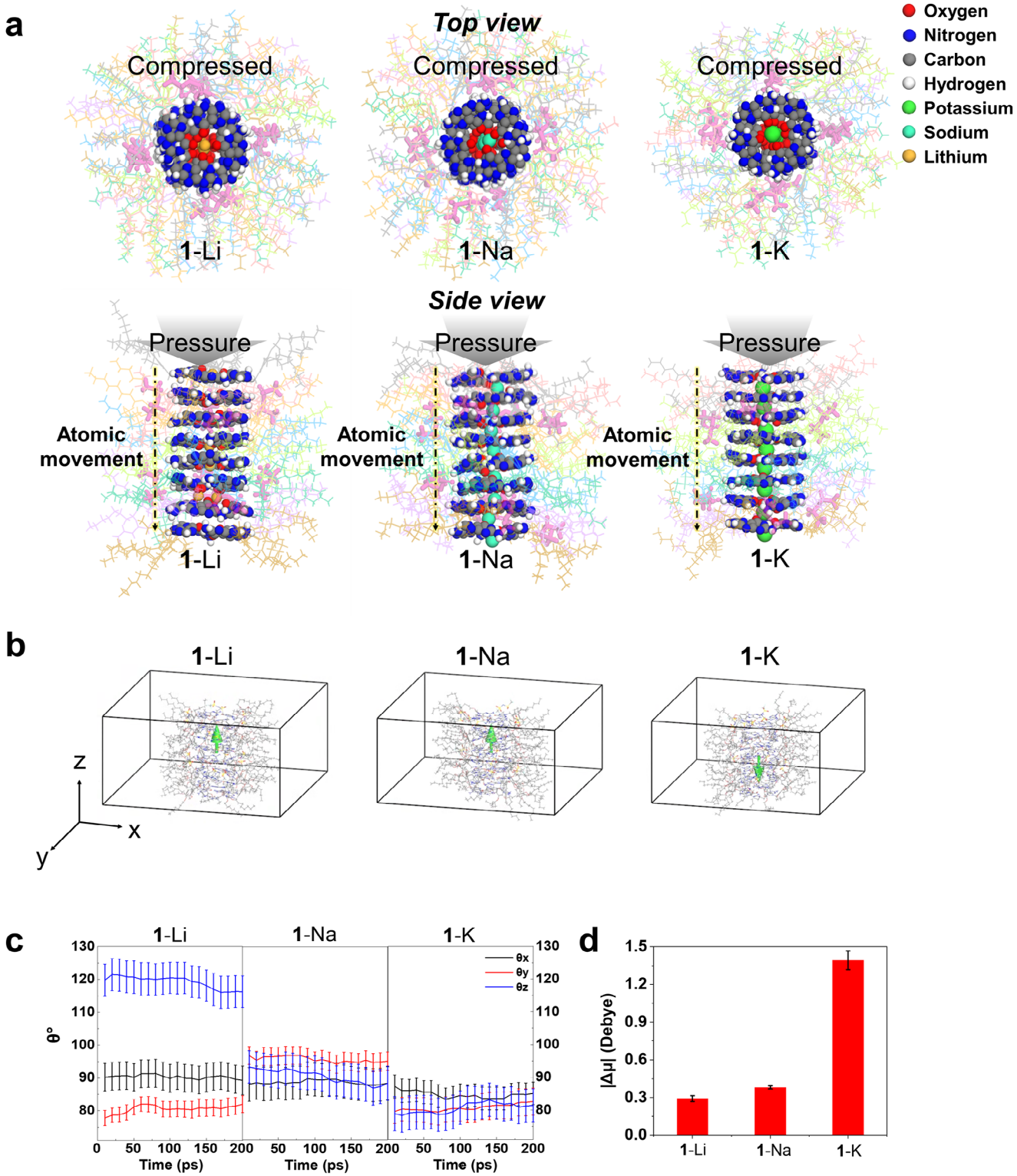

Figure 4. Theoretical analysis of the piezoelectric effect of GQs. a) Top and side views of the compressed system after 200 ps for 1-Li, 1-Na, and 1-K. The alkyl groups are represented by colored lines, and the $TFSI^-$ ions are colored in pink. The guanine of GQs is represented in the CPK model. The grey arrows mean the direction of compression, and the black dot arrows stand for the movement direction of all atoms in GQ complexes. b) The difference of dipole moment vectors between the relaxed and compressed system along the z-axis direction, which are illustrated by green arrows. c) The angles between the net dipole moment vector and *x*-, *y*-, and *z*- axes (i.e., θ_x, θ_y, θ_z), respectively. d) The magnitude of the variable of the net dipole moment vector ($|\Delta\mu|$) between the relaxed and compressed systems. Note that the calculated values are averages of 10 independent simulations for each system.

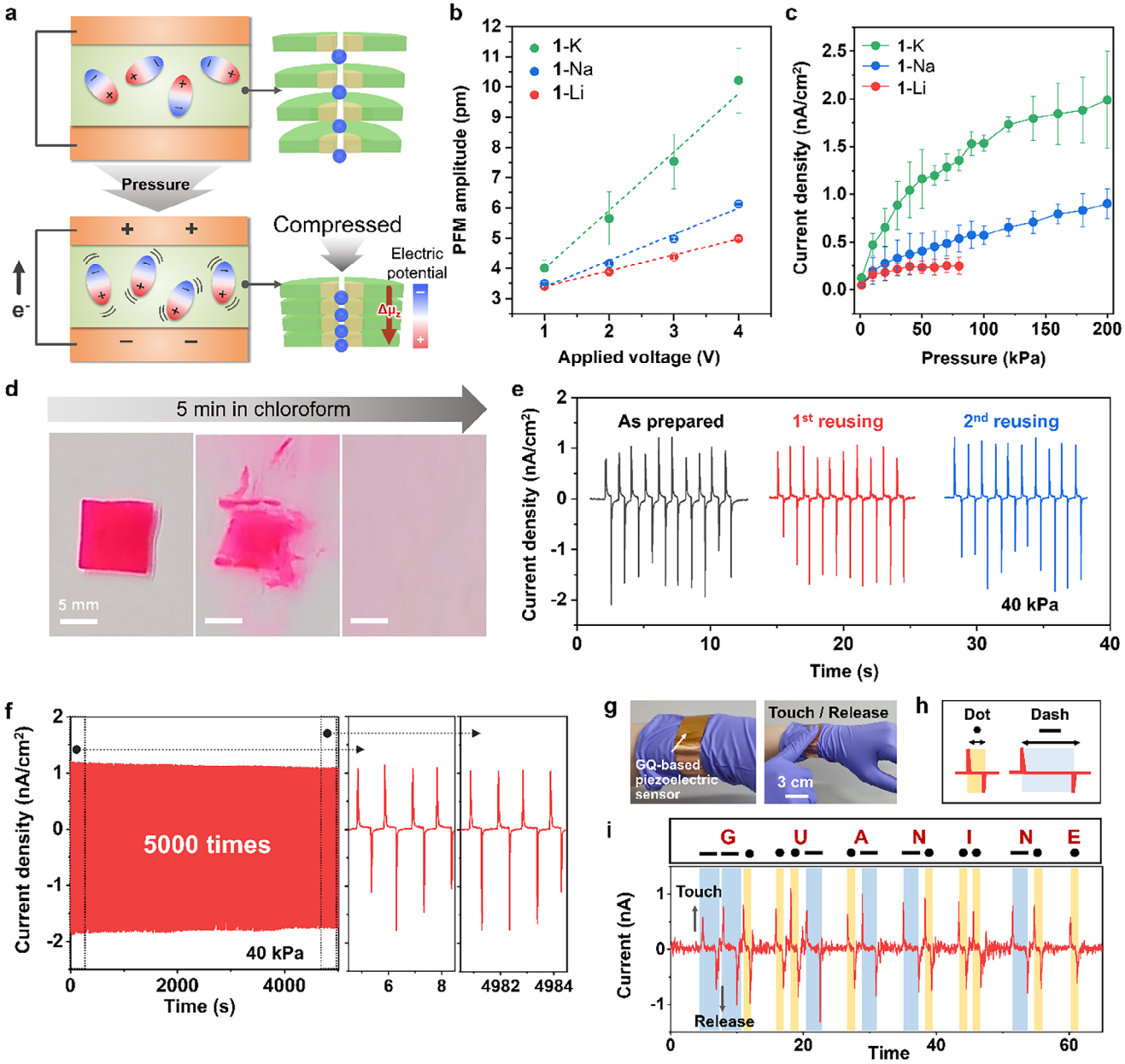

Figure 5. Characterization and application of GQ complex-based piezoelectric sensors. a) Schematic configuration of the piezoelectric performance from the device incorporating the GQ complex. b) PFM amplitude as a function of the applied voltage. c) Piezoelectric current densities as a function of applied pressure. d) Time-lapse photographic images showing dissolution of the GQ complex containing red dye in chloroform over 5 min. e) Piezoelectric current output under 40 kPa for as-prepared (black), 1st reuse (red), 2nd reuse (blue) cycles. f) Stability test showing 5000 cycles of 1-K under 40 kPa. g) Photographic images of the wrist-mounted sensor. h,i) Corresponding sensor output demonstrating Morse code detection of the word "GUANINE". Error bars in (b) and (c) denote the standard deviation from five and three different samples, respectively.

loading–unloading cycles at 40 kPa (Figure 5f), thereby demonstrating its robustness and reliability for practical applications. As a proof-of-concept, the sensor was mounted on the wrist to detect Morse code signals (Figure 5g). Short and long touches were used to represent "Dot" and "Dash", respectively (Figure 5h), enabling the electrical encoding of the word "GUANINE" (Figure 5i). These results highlight the potential of GQ complexes as flexible and recyclable piezoelectric materials for wearable electronics.

3. Conclusion

This study presents the first demonstration of piezoelectric behavior in guanine-quadruplex (GQ) structures formed via ion-mediated self-assembly of amphiphilic guanine derivatives. The incorporation of alkali metal ions (Li^+, Na^+, K^+) not only drives the formation of GQ complexes but also enables facile tunability of piezoelectric response through ion selection, with K^+-assembled structures exhibiting the highest dipole variation

and current output, as confirmed by both simulations and experiments. The resulting GQ-based devices are readily recyclable via a simple dissolution–evaporation process, maintaining performance across repeated cycles. This combination of ion-tunable performance and solvent-assisted recyclability offers a sustainable and versatile alternative to conventional fluorinated piezoelectric polymers. Furthermore, the practical functionality of the devices was demonstrated in wearable Morse-code signal detection, underscoring their applicability in eco-friendly, next-generation bioelectronic platforms and human-machine interfaces.

4. Experimental Section

Preparation of GQ Complexes: Amphiphilic guanine derivative 1 was synthesized following the synthetic procedure detailed in the Supporting Information. GQ complexes were obtained by adding excess salts (MTFSI, M = Li, Na, and K) to 100 mg mL^{-1} solution of molecule 1 in chloroform. After stirring for one day to allow GQ formation, the excess salts were removed using syringe filters. The resulting solution was then evaporated slowly in a dry atmosphere for one day and further dried under vacuum for another day to obtain solid GQ complexes, labeled as 1-Li, 1-Na, and 1-K.

Fabrication of GQ-Based Piezoelectric Device: A 1.0 × 1.0 cm^2 hole was punched through Kapton double-sided tape to serve as an insulating spacer and was attached to a copper electrode. The hole was filled with the GQ complex and covered with another copper electrode to create a sandwich-structured device. In order to reduce the interfacial resistance between the GQ complex and the electrode, the device was fixed with a binder clip, annealed at 150 °C, and then cooled to room temperature.

Characterization: The synthesized molecules and complexes were characterized using 400 MHz nuclear magnetic resonance (NMR) spectroscopy (400-MR DD2, Agilent and AVANCE III HD, Bruker), gel permeation chromatography (1260 Infinity GPC, Agilent), differential scanning calorimetry (Q200, TA Instruments), and Fourier-transform infrared (FT-IR) spectroscopy (Spectrum Two, PerkinElmer). Solid-state ^{1}H MAS NMR experiments were performed using a 600 MHz NMR spectroscopy (VN-MRS600, Agilent) with a 1.6 mm HXY fast MAS triple-resonance probe. Synchrotron WAXD measurements were performed at PLS-II 6D UNIST-PAL beamline (Pohang Accelerator Laboratory, Korea) using 11.564 keV X-rays and a 2D charge-coupled device (CCD) detector (SX165, Rayonix) with a 220 mm sample-to-detector distance. The piezoelectric coefficient was evaluated using atomic force microscopy (AFM, Park NX20, Park Systems). Short-circuit current was measured using a source meter (S-2450, Keithley) under periodic pressure applied by a custom-built pushing tester (Tera Leader, Korea). A pushing tip (area of 5 × 5 mm^2) applied repeated loading at a speed of 600 mm s^{-1} with a delay of 0.5 s. Piezoelectric behavior was confirmed by observing the reverse of current peaks upon switching electrode polarity (forward: ground on top, reverse: ground on bottom).

Simulation Details: To construct the GQ structure, energetically favorable configurations of pairly stacked G-quartets were investigated by the MM simulation[58] using the COMPASSII forcefield.[59] Three variables were chosen: stacking direction, rotation angle, and stacking distance[60] (Figure S9, Supporting Information); opposite directions of stackings could produce head-head and head-trail configurations, the azimuthal angle was changed by rotating the top G-quartet by 10° interval till 90°, and the stacking distance was changed from 3.0 to 4.2 Å by 0.2 Å interval. The formation energy (ΔE_{form}) is calculated as follows,

$$\Delta E_{form} = E_{total} - E_{top} - E_{bottom} - nE_x \quad (1)$$

where E_{total} is the energy of the total system, E_{top} and E_{bottom} are the energy of the top and bottom G-quartet, respectively, n is the number of central metal atoms, and E_x is the energy of the metal atom (i.e., x = Li, Na, and K).

Based on the stable configuration of the pairly stacked G-quartets found from the MM simulation (e.g., for Li, head-tail direction, 20° rotation, and the stacked distance of 3.4 Å), the model system of GQ structure was constructed with stacked 8 G-quartets with $TFSI^-$ ions in the box 60 × 60 × 27.2 $Å^3$ (Figure S10, Supporting Information). Note that metal atoms were accordingly charged in the system (i.e., Li^+, Na^+, and K^+). The atomistic interactions were described by the AMBER force field in the GROMACS 2020.2 program.[61] Specifically, the antechamber program was used to generate interaction parameters of the G-quadruplex.[62,63] The short-range non-bonding interactions were calculated within the cut-off distance of 12 Å, and the particle mesh Ewald (PME) summation was used to calculate electrostatic interactions. To relax the initial system, the MD simulation with the anisotropic NPT (i.e., isothermal-isobaric in z-axis) ensemble was performed for 1 ns at 298 K and 1 atm.[64] To study the piezoelectric effect, the relaxed systems were compressed in the z-axis at the rate of 1 nm ns^{-1} for 200 ps, where the volume was reduced by ≈7% and the maximum pressure was estimated to be no greater than ≈1600 bar at 200 ps. The net dipole moment vector (μ) was calculated using the following equation:[65]

$$\mu = \sum \left(r_i - r_{ref} \right) q_i \quad (2)$$

where r_i is a position vector of the i^{th} atom, r_{ref} is the reference vector (i.e., origin), and q_i is the charge of the i^{th} atom. To quantify the orientation of the net dipole moment vector, the angles (θ_a) between the net dipole moment vector and x-, y-, or z- axes were calculated as follows:

$$\vartheta_a = cos^{-1} \left(\mu_a / |\mu| \right) (a = x, y, z) \quad (3)$$

where μ_a (a = x, y, z) is the net dipole moment vector of a-axes and $|\mu|$ is the magnitude of the net dipole moment vector.

After compression, the direction and magnitude of the net dipole moment were analyzed up to 200 ps, and the induced dipole moment was estimated by the difference between the relaxed and compressed systems. Note that the model system was considered stable if the variation in the distances among the four oxygen atoms within the guanine bases of the G-quartet remained within 5% throughout the 200 ps simulation (Figure S11, Supporting Information).

Supporting Information

Supporting Information is available from the Wiley Online Library or from the author.

Acknowledgements

S.L., S.N., and Y.C. contributed equally to this work. Synchrotron WAXD experiments were supported at PLS-II 6D UNIST-PAL beamlines of Pohang Accelerator Laboratory in Korea. This study contains the results obtained by using the equipment of UCRF (UNIST Central Research Facilities). This work was supported by the National Research Foundation of Korea (NRF) grants funded by the Korean Government (MSIP) (RS-2021-NR059784, RS-2024-00410962, 2020M3A9D8038192, and RS-2023-00257666). Computational resources were from KISTI-HPC (KSC-2023-CRE-0495) and UNIST-HPC.

Conflict of Interest

The authors declare no conflict of interest.

Data Availability Statement

The data that support the findings of this study are available from the corresponding author upon reasonable request.

Keywords

biomaterial, piezoelectric, recyclable, self-assembly, tunability

Received: July 14, 2025
Revised: July 31, 2025
Published online:

[1] J. H. Lee, K. H. Cho, K. Cho, *Adv. Mater.* **2023**, *35*, 2209673.
[2] Y. Hu, Z. L. Wang, *Nano Energy* **2015**, *14*, 3.
[3] H. Wei, H. Wang, Y. Xia, D. Cui, Y. Shi, M. Dong, C. Liu, T. Ding, J. Zhang, Y. Ma, *J. Mater. Chem. C* **2018**, *6*, 12446.
[4] L. Persano, C. Dagdeviren, Y. Su, Y. Zhang, S. Girardo, D. Pisignano, Y. Huang, J. A. Rogers, *Nat. Commun.* **2013**, *4*, 1633.
[5] J. Park, M. Kim, Y. Lee, H. S. Lee, H. Ko, *Sci. Adv.* **2015**, *1*, 1500661.
[6] H. Gullapalli, V. S. Vemuru, A. Kumar, A. Botello-Mendez, R. Vajtai, M. Terrones, S. Nagarajaiah, P. M. Ajayan, *Small* **2010**, *6*, 1641.
[7] Y. Peng, J. Lu, D. Peng, W. Ma, F. Li, Q. Chen, X. Wang, J. Sun, H. Liu, C. Pan, *Adv. Funct. Mater.* **2019**, *29*, 1905051.
[8] Y. H. Jung, T. X. Pham, D. Issa, H. S. Wang, J. H. Lee, M. Chung, B.-Y. Lee, G. Kim, C. D. Yoo, K. J. Lee, *Nano Energy* **2022**, *101*, 107610.
[9] Z. Yang, S. Zhou, J. Zu, D. Inman, *Joule* **2018**, *2*, 642.
[10] K. Dong, X. Peng, Z. L. Wang, *Adv. Mater.* **2020**, *32*, 1902549.
[11] Y. H. Jung, S. K. Hong, H. S. Wang, J. H. Han, T. X. Pham, H. Park, J. Kim, S. Kang, C. D. Yoo, K. J. Lee, *Adv. Mater.* **2020**, *32*, 1904020.
[12] X. Wan, H. Cong, G. Jiang, X. Liang, L. Liu, H. He, A. C. S. Appl, *Nano Mater* **2023**, *6*, 1522.
[13] J. Chen, C. Ayranci, T. Tang, *Mater. Today Chem* **2023**, *30*, 101571.
[14] L. Lu, W. Ding, J. Liu, B. Yang, *Nano Energy* **2020**, *78*, 105251.
[15] A. G. Veiga, F. G. d. A. Dias, L. d. N. Batista, M. L. M. Rocco, M. F. Costa, *Mater. Today Commun.* **2020**, *25*, 101269.
[16] K. Kim, M. Ha, B. Choi, S. H. Joo, H. S. Kang, J. H. Park, B. Gu, C. Park, C. Park, J. Kim, *Nano Energy* **2018**, *48*, 275.
[17] D. Kim, S. A. Han, J. H. Kim, J. H. Lee, S. W. Kim, S. W. Lee, *Adv. Mater.* **2020**, *32*, 1906989.
[18] M. T. Chorsi, E. J. Curry, H. T. Chorsi, R. Das, J. Baroody, P. K. Purohit, H. Ilies, T. D. Nguyen, *Adv. Mater.* **2019**, *31*, 1802084.
[19] R. Wang, J. Sui, X. Wang, *ACS Nano* **2022**, *16*, 17708.
[20] S. Maiti, S. K. Karan, J. K. Kim, B. B. Khatua, *Adv. Energy Mater.* **2019**, *9*, 1803027.
[21] V. Lemanov, *Ferroelectrics* **2000**, *238*, 211.
[22] V. Lemanov, S. Popov, G. Pankova, *Phys. Solid State* **2011**, *53*, 1191.
[23] V. Vivekananthan, N. R. Alluri, Y. Purusothaman, A. Chandrasekhar, S. Selvarajan, S.-J. Kim, *ACS Appl. Mater. Interfaces* **2018**, *10*, 18650.
[24] M. Andonegi, A. G. Diez, C. M. Costa, K. N. Romanyuk, A. L. Kholkin, K. de la Caba, P. Guerrero, S. Lanceros-Mendez, *Int. J. Biol. Macromol.* **2025**, *309*, 142799.
[25] I. Bdikin, A. Heredia, S. M. Neumayer, V. S. Bystrov, J. Gracio, B. J. Rodriguez, A. L. Kholkin, *J. Appl. Phys.* **2015**, *21*, 118.
[26] M. T. Chorsi, T. T. Le, F. Lin, T. Vinikoor, R. Das, J. F. Stevens, C. Mundrane, J. Park, K. T. Tran, Y. Liu, *Sci. Adv.* **2023**, *9*, adg6075.
[27] Y. Wang, S. Liu, L. Li, H. Li, Y. Yin, S. Rencus-Lazar, S. Guerin, W. Ouyang, D. Thompson, R. Yang, *J. Am. Chem. Soc.* **2023**, *145*, 15331.
[28] S. Bera, S. Guerin, H. Yuan, J. O'Donnell, N. P. Reynolds, O. Maraba, W. Ji, L. J. Shimon, P.-A. Cazade, S. A. Tofail, *Nat. Commun.* **2021**, *12*, 2634.
[29] H. Yuan, P. Han, Z. Tao, B. Xue, Y. Guo, D. Levy, W. Hu, Y. Wang, Y. Cao, E. Gazit, *ACS Appl. Mater. Interfaces* **2022**, *14*, 6538.
[30] X. Liang, H. Xu, H. Cong, X. Wan, L. Liu, Y. Li, C. Liu, C. Chen, G. Jiang, K. Asadi, *ACS Appl. Mater. Interfaces* **2023**, *15*, 55790.
[31] E. Kar, M. Barman, S. Das, A. Das, P. Datta, S. Mukherjee, M. Tavakoli, N. Mukherjee, N. Bose, *Sustain. Energ. Fuels* **2021**, *5*, 1857.
[32] Z. Zhang, X. Li, Z. Peng, X. Yan, S. Liu, Y. Hong, Y. Shan, X. Xu, L. Jin, B. Liu, *Nat. Commun.* **2023**, *14*, 4094.
[33] A. Ramesh, T. N. Das, T. K. Maji, G. Ghosh, *Chem. Sci.* **2024**, *15*, 16355.
[34] I. Terzic, N. L. Meereboer, M. Acuautla, G. Portale, K. Loos, *Nat. Commun.* **2019**, *10*, 601.
[35] D. Gupta, V. Gupta, D. Nath, C. Miglani, D. Mandal, A. Pal, *ACS Appl. Mater. Interfaces* **2022**, *15*, 25110.
[36] Q. He, Y. Zeng, L. Jiang, Z. Wang, G. Lu, H. Kang, P. Li, B. Bethers, S. Feng, L. Sun, *Nat. Commun.* **2023**, *14*, 6477.
[37] K. G. Zyner, A. Simeone, S. M. Flynn, C. Doyle, G. Marsico, S. Adhikari, G. Portella, D. Tannahill, S. Balasubramanian, *Nat. Commun.* **2022**, *13*, 142.
[38] J.-L. Mergny, D. Sen, *Chem. Rev.* **2019**, *119*, 6290.
[39] J. T. Davis, *Angew. Chem., Int. Ed.* **2004**, *43*, 668.
[40] E. Largy, J.-L. Mergny, V. Gabelica, *Met. Ions Life Sci.* **2016**, *16*, 203.
[41] B. Pagano, A. Randazzo, I. Fotticchia, E. Novellino, L. Petraccone, C. Giancola, *Methods* **2013**, *64*, 43.
[42] M. L. Bochman, K. Paeschke, V. A. Zakian, *Nat. Rev. Genet.* **2012**, *13*, 770.
[43] H. M. Wong, L. Payet, J. L. Huppert, *curr. Opin. Mol. ther* **2009**, *11*, 146.
[44] D. J. Patel, A. T. n. Phan, V. Kuryavyi, *Nucleic Acids Res.* **2007**, *35*, 7429.
[45] J. W. Shim, Q. Tan, L.-Q. Gu, *Nucleic Acids Res.* **2009**, *37*, 972.
[46] C. J. Lech, B. Heddi, A. T. Phan, *Nucleic Acids Res.* **2013**, *41*, 2034.
[47] D. Pavc, B. Wang, L. Spindler, I. Drevenšek-Olenik, J. Plavec, P. Šket, *Nucleic Acids Res.* **2020**, *48*, 2749.
[48] J. L. Sessler, M. Sathiosatham, K. Doerr, V. Lynch, K. A. Abboud, *Angew. Chem., Int. Ed.* **2000**, *39*, 1300.
[49] D. González-Rodríguez, J. L. Van Dongen, M. Lutz, A. L. Spek, A. P. Schenning, E. Meijer, *Nat. Chem.* **2009**, *1*, 151.
[50] G. Wu, I. C. Kwan, *J. Am. Chem. Soc.* **2009**, *131*, 3180.
[51] G. M. Reddy, A. Huqi, D. Iuga, S. Sakurai, A. Marsh, J. T. Davis, S. Masiero, S. P. Brown, *Chem. – Eur. J.* **2017**, *23*, 2315.
[52] S.-K. Cho, K. M. Lee, S.-H. Kang, K. Jeong, S.-P. Han, J. E. Lee, S. Lee, T. J. Shin, J.-H. Ryu, C. Yang, *Sci. Adv.* **2022**, *8*, abp8751.
[53] A. Blanco, G. Blanco, *Medical Biochemistry*, Academic Press, Cambridge, Massachusetts **2017**.
[54] M. Mizuno, *Encyclopedia of Thermal Stresses*, Springer, Netherlands **2014**, 3728.
[55] X. Ren, H. Fan, Y. Zhao, Z. Liu, *ACS Appl. Mater. Interfaces* **2016**, *8*, 26190.
[56] S. D. Mahapatra, P. C. Mohapatra, A. I. Aria, G. Christie, Y. K. Mishra, S. Hofmann, V. K. Thakur, *Adv. Sci.* **2021**, *8*, 2100864.
[57] H. K. Ravi, F. Simona, J. r. Hulliger, M. Cascella, *J. Phys. Chem. B* **2012**, *116*, 1901.
[58] H. Sun, Z. Jin, C. Yang, R. L. Akkermans, S. H. Robertson, N. A. Spenley, S. Miller, S. M. Todd, *J. mol. model.* **2016**, *22*, 47.
[59] Dassault Systèmes Biovia, *Materials Studio*, Dassault Systèmes, San Diego, CA **2023**.
[60] S. H. Kang, K. M. Lee, S. K. Cho, J. E. Lee, D. Won, S. Y. Lee, S. K. Kwak, C. Yang, *ChemSusChem* **2022**, *15*, 202102201.
[61] D. Van Der Spoel, E. Lindahl, B. Hess, G. Groenhof, A. E. Mark, H. J. Berendsen, *J. Comput. Chem.* **2005**, *26*, 1701.
[62] J. Wang, W. Wang, P. A. Kollman, D. A. Case, *J. mol. graph. modell.* **2006**, *25*, 247.
[63] J. Wang, R. M. Wolf, J. W. Caldwell, P. A. Kollman, D. A. Case, *J. Comput. Chem.* **2004**, *25*, 1157.
[64] A. Krishnan, D. Dhamodharan, T. Sundaram, V. Sundaram, H.-S. Byun, *Korean J. Chem. Eng.* **2022**, *39*, 1368.
[65] H. M. Lee, Y. W. Kim, E. M. Go, C. Revadekar, K. H. Choi, Y. Cho, S. K. Kwak, B. J. Park, *Nat. Commun.* **2023**, *14*, 3838.